

High-mobility, low-resistive boron-doped diamond material realized by oxygen assistance

Gengyou Zhao(赵耕右), Kun Tang(汤琨), Kai Yang(杨凯), Bo Feng(冯博), Liangxue Gu(顾梁雪), Xiang Xiong(熊翔), Tao Tao(陶涛), Bin Liu(刘斌), Jiandong Ye(叶建东), Rong Zhang(张荣), Youdou Zheng(郑有炓), and Shulin Gu(顾书林)

Citation: Chin. Phys. B, 2026, 35 (**4**): 048101. DOI: 10.1088/1674-1056/ae0636
http://cpb.iphy.ac.cn; http://iopscience.iop.org/cpb

What follows is a list of articles you may be interested in

Regulation mechanism of Si vacancies in unintentional silicon-doped diamond by gas flow in MPCVD

Kai Yang(杨凯), Liangxue Gu(顾梁雪), Gengyou Zhao(赵耕右), Kun Tang(汤琨), Bo Feng(冯博), Jiandong Ye(叶建东), Rong Zhang(张荣), Shunming Zhu(朱顺明), and Shulin Gu(顾书林)

Chin. Phys. B, 2025, 34 (**11**): 118102. DOI: 10.1088/1674-1056/ae07aa

Effect of metal solvent and growth surface on boron doping efficiency and impurity incorporation in HPHT-grown diamond single crystals

Hongbo Li(李鸿波), Wenhao Wang(王文豪), Yadong Li(李亚东), Liangchao Chen(陈良超), Zhuangfei Zhang(张壮飞), Yuewen Zhang(张跃文), Qianqian Wang(王倩倩), Biao Wan(万彪), Chunlei Du(杜春雷), and Chao Fang(房超)

Chin. Phys. B, 2025, 34 (**11**): 118101. DOI: 10.1088/1674-1056/adfb55

Synthesis of two-dimensional diamond by phase transition from graphene at atmospheric pressure

Songyang Li(李松洋), Zhiguang Zhu(朱志光), Youzhi Zhang(张有志), Chengke Chen(陈成克), and Xiaojun Hu(胡晓君)

Chin. Phys. B, 2025, 34 (**5**): 058101. DOI: 10.1088/1674-1056/adb688

Pressure generation under deformation in a large-volume press

Saisai Wang(王赛赛), Xinyu Zhao(赵鑫宇), Kuo Hu(胡阔), Bingtao Feng(丰丙涛), Xuyuan Hou(侯旭远), Yiming Zhang(张羿鸣), Shucheng Liu(刘书成), Yuchen Shang(尚宇琛), Zhaodong Liu(刘兆东), Mingguang Yao(姚明光), and Bingbing Liu(刘冰冰)

Chin. Phys. B, 2024, 33 (**9**): 098104. DOI: 10.1088/1674-1056/ad58c6

Synthesis and nitrogen content regulation of diamond in a high-pressure hydrogen-rich environment

Guofeng Huang(黄国锋), Liangchao Chen(陈良超), and Chao Fang(房超)

Chin. Phys. B, 2024, 33 (**6**): 068102. DOI: 10.1088/1674-1056/ad2a6d

---

High-mobility, low-resistive boron-doped diamond material realized by oxygen assistance

Gengyou Zhao(赵耕右)[1,2], Kun Tang(汤琨)[1,2,†], Kai Yang(杨凯)[1,2], Bo Feng(冯博)[1,2], Liangxue Gu(顾梁雪)[1,2], Xiang Xiong(熊翔)[3], Tao Tao(陶涛)[1,2], Bin Liu(刘斌)[1,2], Jiandong Ye(叶建东)[1,2], Rong Zhang(张荣)[1,2], Youdou Zheng(郑有炓)[1,2], and Shulin Gu(顾书林)[1,2,‡]

[1] *School of Electronic Science and Engineering, Nanjing University, Nanjing* 210046, *China*
[2] *Jiangsu Key Laboratory of Advanced Semiconductors and High Energy-Efficiency Devices, Nanjing* 210046, *China*
[3] *School of Physics, Nanjing University, Nanjing* 210008, *China*

(Received 7 July 2025; revised manuscript received 11 September 2025; accepted manuscript online 12 September 2025)

The effect of trace oxygen on the light-doping behavior of boron in diamond films during microwave plasma chemical vapor deposition was experimentally investigated. Boron-doped diamond films were grown continuously under different oxygen concentrations [oxygen/carbon (O/C) = 0%–5%]. When oxygen was added during the diamond doping process, improvements in crystal quality and surface morphology were observed, and residual nitrogen was significantly suppressed. However, further increasing the oxygen concentration could lead to surface defects. We evaluated and discussed the carrier mobility, carrier concentration and boron content of the samples. At room temperature, under the condition of O/C = 4%, the maximum hole mobility reached 1400 $cm^2 \cdot V^{-1} \cdot s^{-1}$, and a higher carrier concentration of 1.5×10^{15} cm^{-3} was obtained, which is an excellent result compared with all previous studies. In addition, the characteristic peaks that appeared in both low-temperature photoluminescence spectra and absorption spectra were analyzed, and it was found that the characteristic peak at 4.7 eV (270 nm) may correspond to a boron–nitrogen complex, supplementing the effect of boron-doped diamond on defect formation. These findings demonstrate the potential of controlling the boron concentration in diamond films using oxygen concentration in a plasma environment and open avenues for future applications in advanced optoelectronic devices.

Keywords: diamond, chemical vapor deposition, impurity concentration, electrical properties, infrared and Raman spectra

PACS: 81.05.ug, 81.15.Gh, 61.72.sd, 87.15.Pc, 78.30.–j

DOI: 10.1088/1674-1056/ae0636 **CSTR:** 32038.14.CPB.ae0636

1. Introduction

Diamond is a wide-bandgap semiconductor that exhibits exceptional properties, such as an ultra-wide bandgap (5.5 eV), extreme hardness (1200 GPa), high electron and hole mobility (4000 $cm^2 \cdot V^{-1} \cdot s^{-1}$), superior thermal conductivity (20 $W \cdot cm^{-1} \cdot K^{-1}$) and a substantial breakdown field strength (10 $MV \cdot cm^{-1}$). It also has perfect chemical stability and is known as the 'ultimate semiconductor material'. These characteristics enable applications in high-temperature, high-frequency, high-voltage and high-power electronic devices.[1–4] Boron-doped single-crystal diamond shows particular promise for advanced power electronics, and precise dopant control is one of the most difficult challenges. Boron is an acceptor in diamond and a carbon atom replaced by a boron atom generates an acceptor level near the top of valence band with an activation energy of 0.37 eV,[5] the shallow acceptor depth of which facilitates p-type conduction in ultra-wide bandgap semiconductors.[6,7] Recent research focusing on high-mobility and high-carrier-concentration boron-doped diamond has gained attention for high-power diamond Schottky diodes.[8] Among various synthesis methods, microwave plasma chemical vapor deposition (MPCVD) technology enables controlled epitaxial growth through modulation by changing the concentration of methane and doping gas and controlling the growth temperature and microwave power. It has been widely employed to grow p-type diamond with high crystal quality and doping concentrations.[9]

Boron doping may induce lattice mismatch and generate defects (dislocations and point defects), which compromise crystal quality and degrade the electrical properties, so highly efficient p-type diamond is still not easy to achieve. The research results of Mortet *et al.*,[10] Yap *et al.*,[11] Volpe *et al.*[9] and Ding *et al.*[12] have shown that it is very difficult to achieve a high hole concentration and high mobility (or high crystal quality) in p-type diamond simultaneously. Co-doping has emerged as a common approach in the growth of wide-bandgap semiconductor materials to maintain high carrier density while having high mobility;[13,14] this enables precise modulation of the dopant population, electronic characteristics and magnetic properties, promotes dopant ioniza-

†Corresponding author. E-mail: ktang@nju.edu.cn
‡Corresponding author. E-mail: slgu@nju.edu.cn

© 2026 Chinese Physical Society and IOP Publishing Ltd. All rights, including for text and data mining, AI training, and similar technologies, are reserved.

tion and restores lattice mismatch. Doping with multiple elements (such as boron with sulfur, phosphorus, nitrogen and oxygen) significantly regulates the growth and material properties of boron-doped diamond and can improve the lattice quality.[4,15–17] These co-dopants act as surfactants at growth interfaces, greatly boosting the efficiency of boron incorporation. Additionally, they regulate surface growth processes including atomic migration, adsorption and desorption. Oxygen merits particular attention due to its plasma etching effect, which demonstrably enhances diamond quality during boron incorporation.[3,18–20] Despite these advances, diamond semiconductors concurrently exhibiting high carrier density and high mobility remain unrealized. Further performance gains may require optimized fabrication processes. Thus, investigating the impact of oxygen on boron-doping behavior is critical for developing high-performance p-type diamond electronic devices. This study explores trace oxygen incorporation during very light boron doping to assess its influence on higher hole concentration and mobility. Successful implementation could advance diamond-based p-channel metal–oxide–semiconductor device technology through superior p-type diamond material.

In this work, we synthesized boron-doped p-type diamond via MPCVD using diborane (B_2H_6) and oxygen (O_2) as the gas sources. We characterized the as-grown diamond films through atomic force microscopy (AFM), Raman scattering spectroscopy, x-ray diffraction (XRD), photoluminescence (PL) spectroscopy, Fourier transform infrared (FTIR) transmission spectra, absorption spectra and Hall effect measurements. We systematically investigated the influence of varying the trace oxygen concentration on surface morphology, crystal quality, luminescence properties, boron doping efficiency and electrical properties in relatively lightly boron-doped diamond films, and simultaneously achieved p-type diamond films with high mobility and carrier concentration. Low-temperature PL and absorption spectra revealed previously unreported defect signatures. The 4.7 eV (270 nm) peak was identified as a boron–nitrogen complex, providing new insights into the defect formation mechanisms in doped diamond.

2. Method

Boron-doped diamonds were fabricated by MPCVD (HMPS-2040SP) on (100)-oriented Ib-type single-crystalline chemical vapor deposition (CVD) diamond substrates (3 mm×3 mm×1 mm). First, the substrate was heated in sulfuric acid and nitric acid ($v(H_2SO_4)$:$v(HNO_3)$ = 3:1) at 300 °C for 1 h to remove non-diamond phases from the surface of the crystalline species. This was followed by sequential ultrasonic rinsing in acetone, ethanol and deionized water (10 min each) to remove organic matter and impurities on the surface, and finally nitrogen drying. During the growth, the flow rates of high-purity CH_4 and H_2 (5N) were maintained at 20 sccm and 500 sccm, respectively. The hydrogen gas flowed through a purifier before entering the reaction chamber. Before the growth, the surface of the substrate was systematically etched with hydrogen plasma for 15 min to remove surface defects. To ensure the incorporation of boron and oxygen, high-purity diborane and oxygen (5N) were used as dopants. The gas phase ratio of B/C was fixed at 5 ppm for all samples. To investigate the effect of trace oxygen on boron-doped diamond films, the oxygen concentration evaluated by the oxygen/carbon (O/C) gas ratio was kept at 0%, 1%, 2%, 3%, 4% and 5%. A molybdenum ring beneath the susceptor minimized heat dissipation, enabling lower microwave power. The chamber pressure and microwave power were maintained at 180 Torr and 3.8 kW, respectively, and the substrate temperature was set to 840 °C as calibrated by an infrared pyrometer. The trace and stable dopant flow rate were regulated using flow controllers with precision valves. After growth for 1 h, samples were washed with aqua regia at 220 °C for 30 min to remove graphitic and metallic contaminants. After chemical treatment, the samples were also rinsed in solvent with acetone, alcohol and deionized water.

After the growth, optical characterization and electrical testing of all samples were required. The mass change was measured using a precision electronic balance and the thickness of the boron-doped film was determined by calibrating the thickness change before and after growth with a spiral micrometer. To investigate the surface morphology of diamond, AFM (NTEGRA) in tapping mode was used to quantify the root mean square (RMS) roughness of the film. Raman scattering spectra and PL spectra were acquired at 100× magnification (numerical aperture = 0.9) using a confocal microscope (Horiba Jobin Yvon) with a 514 nm laser as the excitation source. The crystalline quality of the grown diamond layer was monitored by XRD (PANalytical). We further used a 213 nm laser (Xiton IMPRESS-213) to record PL spectra at 10 K for analyzing the concentration of boron-bound excitons and other defects. The characteristic absorption (Cary 5000) peaks obtained from absorption spectra could confirm the defect shown by low-temperature PL. FTIR (Nicolet iS50 FT-IR) could estimate the boron concentration in the epilayer, which was compared with the concentration of boron-bound excitons. Hall effect measurements (HL5500PC) were performed at room temperature (300 K) using the van der Pauw configuration to determine the electrical properties (hole concentration and mobility) of the films. The electrode material consisting of Ti/Au (50 nm/100 nm) was prepared by electron beam evaporation (DE500CL) on the four corners of the sample. The plated electrode sample was annealed at 500 °C in a vacuum environment for 30 min.

3. Results and discussion

In this work, the surface morphology, defect density and crystal quality of lightly boron-doped diamond films were modulated by controlling the O/C ratio. Figure 1 reveals a non-monotonic dependence of the diamond growth rate on the O/C ratio. We also used a precision electronic balance to obtain the mass change to compensate for the error; the mass changes and the film thickness converted from mass change caused by different O/C ratios are plotted in Fig. S1. It can be seen that the growth rate increases from 6 μm·h^{-1} to 9 μm·h^{-1} with the initial introduction of oxygen (O/C $< 3\%$), but declines to 5 μm·h^{-1} at O/C $= 5\%$. The kinetic mechanism involves dual roles for oxygen. When there is a small amount of oxygen in the plasma, microwave energy cracks O_2 into free radicals (such as OH, O, etc.), catalyzing methane decomposition.[21] This elevates the concentration of C_2 species in the plasma, accelerating carbon deposition. At high O/C ratios, excess oxygen exhibits hydrogen-like etching behavior,[16] resulting in a reduction in the carbon deposition rate. Excess oxygen induces the concentration of methyl radicals, which further inhibits diamond growth.[22]

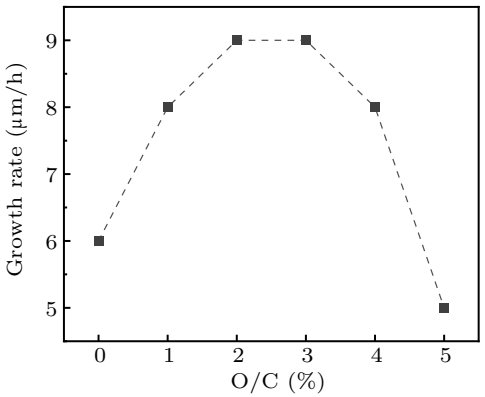


Fig. 1. The growth rate of boron-doped diamond films varies with increase in the O/C gas ratio.

AFM images (10 μm×10 μm scan area) reveal oxygen-dependent evolution of surface features in lightly boron-doped diamond films with corresponding RMS roughness (Fig. 2). We provide two additional scans from different areas of the same sample to confirm consistency with data reported in the literature and plot them in Fig. S2. We calculated the average RMS from three different scan areas of the same sample and plot them in Fig. 2(b), adding an error bar for each result. All samples exhibit stripe-like growth hillocks and non-epitaxial crystalline particles — characteristic morphological defects in homoepitaxial CVD diamond. The striped hillocks grown on (100) epitaxial CVD diamond layers are attributed to nucleation at surface defects or repeated two-dimensional nucleation,[23] which initiate nucleation at interfacial stacking faults or dislocations.[24,25] Atomic steps will be generated on the (100) surface of epitaxial CVD diamond and macroscopic steps will be formed when radical surface diffusion rates match step advancement.[26] The two-dimensional nuclei will coalesce into a larger step and form a hierarchical spiral structure to produce striped hillocks.[27] Concurrently observed "inverted pyramid" etching pits in the surface film correlate with critical plasma chemistry.[28] Boron monodoped film (O/C $= 0\%$) shows abundant etch pits and large streak hillocks caused by threading dislocations induced during the growth process.[29] With the addition of oxygen, the RMS roughness (Rq) decreases from 3.07 nm (O/C $= 0\%$) to 0.64 nm (O/C $= 1\%$), indicating that the surface quality is improved. Since the etching rate of trace oxygen free radicals is faster than that of hydrogen and the surface defects of diamond formed during the diamond growth process will be easily etched by oxygen free radicals,[30] this could form an atomically smooth surface morphology. Excess oxygen can accelerate surface etching and doping with more oxygen atoms produces lattice distortion, thereby reducing surface quality. As the O/C ratio gradually increases to 5%, the RMS roughness of the diamond sample due to etching also gradually increases to 3.12 nm. However, a smaller roughness ($Rq = 1.45$ nm) appears under the condition O/C $= 4\%$, which may be related to the small number of defects and high lattice quality of the sample. For the sample with O/C $= 1\%$, a very high surface quality is obtained, with few hillocks and etching pits seen on the grown surface.

The Raman spectrum obtained from the diamond films is shown in Fig. 3(a); we measure two additional Raman spectra for each sample and plot them in Fig. S3. Figure 3(b) plots the average full width at half maximum (FWHM) of the three times diamond characteristic peak at 1333 cm^{-1}.[31] In Fig. 3(a), all samples exhibit the characteristic diamond peak at 1333 cm^{-1} with no detectable G peak ($\sim$ 1550 cm^{-1}) in the 1500–1700 cm^{-1} range,[32] confirming the absence of graphitic phases. The FWHM of the diamond characteristic peak, quantified in Fig. 3(b), demonstrates a strong correlation with AFM RMS roughness trend,[27] indicating the synchronized impact of oxygen on lattice quality and surface morphology. Therefore, minimal FWHM values at oxygen concentrations of 1% and 4% signify optimal crystal quality, where trace oxygen can balance the lattice mismatch caused by boron doping and mitigate boron-induced lattice strain.[21] We find that oxygen-deficient conditions (O/C $= 0\%$) yield lower growth rates without quality improvement, while excess oxygen (O/C $= 5\%$) causes lattice distortion through violent etching and substitutional defects, which cause lattice mismatch and reduce lattice quality. The broad peak around 1420 cm^{-1} corresponds to luminescence from NV^0 centers,[31,33] as shown in Fig. 3(c). We use the characteristic peak intensity of 1420 cm^{-1} to calculate the content of nitrogen vacancies in the boron-doped diamond film, as plotted in the upper right corner of Fig. 3(c). It can be seen that trace oxygen inhibits nitrogen-related defects, whereas excess oxygen promotes their formation.

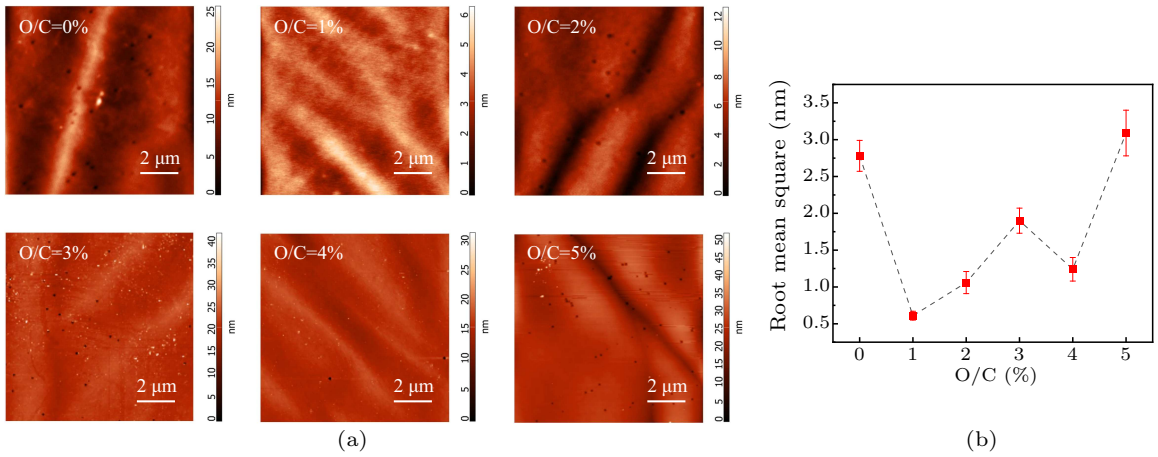


Fig. 2. (a) AFM images of boron-doped diamond films under different oxygen concentrations. (b) Variation diagram of the averaged root mean square *Rq* of boron-doped diamond under different oxygen concentrations.

The Raman spectrum peak shifts relative to the standard diamond peak (1333 cm^{-1}) revealing the evolution of doping-induced stress in the lattice structure caused by boron and oxygen doping.[26,34] The change of stress in the film can be quantified through biaxial stress approximation using the formula $\sigma = -0.567(\upsilon_m - \upsilon_0)$,[35,36] where υ_0 denotes the stress-free reference (1333 cm^{-1}) and υ_m represents measured peak positions, noting that compressive and tensile stresses, respectively, induce higher and lower frequency shifts.[37] We analyze the characteristic Raman peak position in Fig. 3(a) and plot it in Fig. 3(d). Systematic analysis of peak positions demonstrates an upward wavenumber shift from 1332.1 cm^{-1} (O/C = 0%) to 1332.5 cm^{-1} (O/C = 2%–4%), corresponding to decreased tensile stress from 0.51 GPa to 0.28 GPa. This indicates that when trace amounts of oxygen are present, the stress in the boron-doped diamond film is very small, and when the oxygen concentration increases it will lead to an increase in the internal tensile stress. The observed stress modulation stems from atomic size disparity: boron atoms (larger than carbon) and oxygen atoms (smaller than carbon) generate intrinsic strain during doping.[35] At low oxygen concentrations, oxygen compensates boron-induced lattice distortion, minimizing net stress changes. However, increasing oxygen incorporation expands the lattice parameter, and increases thermal stress at the film–substrate interface.[36]

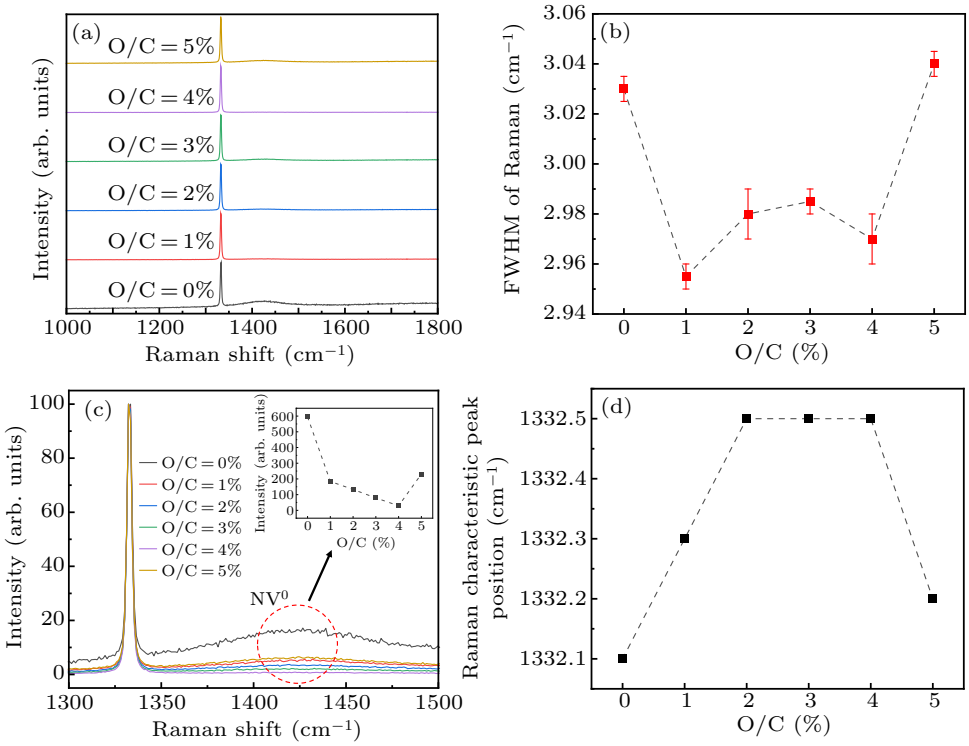


Fig. 3. Raman characterization results of boron-doped diamond films with increasing O/C ratio: (a) Raman spectra of boron-doped diamond films; (b) the averaged FWHM of the Raman scattering peak of diamond as a function of O/C ratio; (c) the characteristic peak of NV^0 in the Raman spectrum (the inset shows the intensity of the 1420 cm^{-1} peak changing with oxygen concentration); (d) Raman characteristic peak position as a function of O/C ratio.

The crystalline quality of boron-doped diamond films is evaluated through XRD rocking curve analysis on the (004) plane (Fig. 4(a)). The x-ray intensity of a single pixel is extracted from the image series scanned by a given rocking curve, and the peak position and width of the pixel are extracted by Gaussian fitting. The x-axis represents the variation of the omega scan ($\Delta\omega$), while the y-axis represents the normalization intensity of the diamond peaks. Figure 4(b) shows the fitted FWHM of the XRD peak as a function of oxygen concentration, indicating that oxygen-assisted growth can improve the crystallinity of diamond,[8] and the best lattice quality (FWHM = 85 arcsec) is obtained at O/C = 4%. Raman analysis provides qualitatively compatible results. The 2θ scan results for all samples are shown in Fig. 4(c). The sole reflection from the (400) Bragg planes confirms single-crystal integrity across all doping conditions and no additional reflections characteristic of polycrystalline diamond growth are observed.[38] Figure 4(d) plots the FWHM of the (400) peaks in the 2θ scan, which is consistent with the rocking curve trend. We plot the shift of the rocking curve peak position with different O/C ratios in Fig. S4; the shift in the rocking curve peak position is due to the mechanical bending of the substrate and crystal. The peak position shifts from 59.42° (O/C = 0%) to a maximum angle of 59.82° (O/C = 3%), and when the oxygen concentration continues to increase to 5% the peak position decreases to 59.71°. Therefore, the difference in peak position can be used as evidence for stress analysis based on the Raman peak shift.

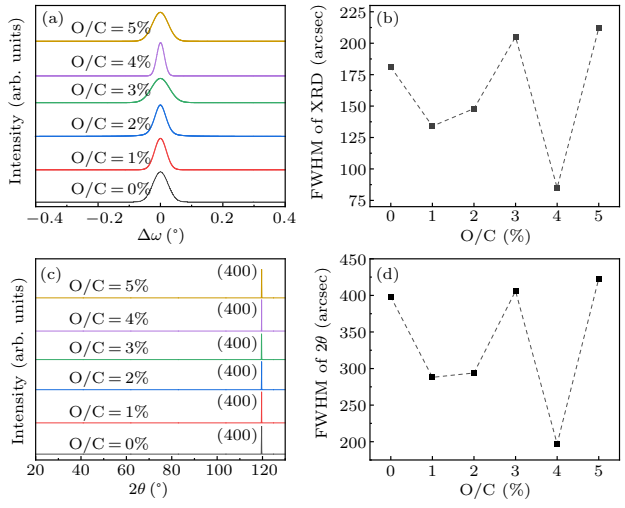


Fig. 4. XRD characterization results of boron-doped diamond films: (a) XRD rocking curves in the (004) plane of boron-doped diamond films; (b) the FWHM of the XRD peak as a function of O/C ratio; (c) the 2θ scan results; (d) the FWHM of 2θ as a function of O/C ratio.

We used PL spectroscopy to investigate defect characteristics and properties of diamond (shown in Fig. 5). We discovered the luminescence of nitrogen vacancies (NVs) in the film. Figure 5(a) shows the PL spectra of all samples (the intensities of NV^0 and NV^- centers have been normalized by the intrinsic peak of diamond). PL of the NVs at 575 nm (NV^0) and 637 nm (NV^-) is ubiquitous in CVD diamond due to residual nitrogen contamination.[39] NV defects may originate from residual nitrogen on the chamber wall or trace nitrogen impurities in the substrate. However, we found that the incorporated residual nitrogen content was almost identical for different runs. Figure S5 shows the PL of three intrinsic diamond samples, and the NV PL intensity is analogous for the three samples. In this case, assuming a similar "dose" of unintentional nitrogen during the growth of the boron-doped samples, the change in the NV luminescence intensity of the currently studied diamond samples should be related to the effect of the oxygen variation. To quantify the effect of oxygen incorporation on the luminescence of NV centers in boron-doped diamond films, the intensities of NV^0, NV^- and $NV^0 + NV^-$ in the PL spectra were extracted, as shown in Fig. 5(b). With an increase in the oxygen concentration, the NV intensity gradually decreases, and the intensity is negligible at O/C = 4%, which corresponds to the better surface morphology and higher lattice quality under this condition. The change in surface and crystalline quality due to oxygen variation could be the reason for the different levels of NV incorporation. The normalized NV intensity is negligible at O/C = 4%, correlating with optimal crystalline quality (XRD FWHM = 85 arcsec) and surface

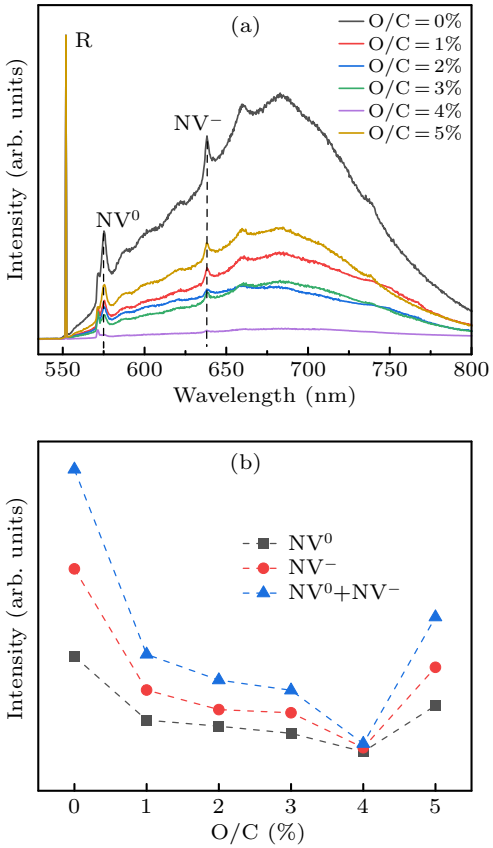


Fig. 5. Effect of oxygen concentration on the density of defects in diamond films obtained from PL spectroscopy: (a) PL spectra of boron-doped diamond films with an excitation wavelength of 514 nm; (b) the intensity of NV^0 and NV^- as a function of the O/C ratio.

smoothness. A trace oxygen plasma etches surface impurities during growth, suppressing nitrogen incorporation pathways.[40] Additionally, reactive oxygen species scavenge residual nitrogen through formation of NO-related gas products, depleting NV precursors.[41] Notably, NV intensity rebounds at O/C = 5% (Fig. 5(b)), coinciding with an unsatisfactory lattice from excessive etching, and defects will be more easily formed. The PL spectrum confirms the changing trend of the characteristic peak intensity at 1420 cm^{-1} in the Raman spectrum, confirming that regulation of nitrogen vacancy formation is dependent on the oxygen concentration.

FTIR spectroscopy can quantify boron incorporation in diamond films. Figure 6(a) illustrates the typical FTIR absorption spectrum of boron-doped diamond film, revealing three characteristic regions: the one-phonon region with N impurity absorption (400–1332 cm^{-1}), two-phonon (1332–2665 cm^{-1}) and three-phonon (2665–4000 cm^{-1}) absorptions.[42] The peak at 2800 cm^{-1}, corresponding to the ground state to second excited state electronic transition of the neutral boron acceptor,[43] serves as a quantitative indicator of doping concentration in the range of 10^{16} cm^{-3} to 10^{18} cm^{-3}.[44] The uncompensated acceptor concentration ($N_a - N_d$) can be evaluated through the established relationship

$$N_a - N_d = 8 \times 10^{17} I_{2800}\ (\mathrm{cm}^{-3}), \tag{1}$$

where I_{2800} is the integrated area of the 0.347 eV peak in the graph of absorption coefficient (α) versus photon energy (in eV).[44] The absorption coefficient is given by $(1/t)\ln A$, where t is the thickness of the diamond film and A is its linear absorption.[45] The relationship between the absorption coefficient and photon energy is shown in Fig. 6(b). Figure 6(c) shows the boron doping concentration in the boron-doped diamond film. Compared with the oxygen-free diamond film, trace oxygen significantly inhibits boron doping efficiency, and the uncompensated acceptor concentration decreases from 3.5×10^{17} cm^{-3} (O/C = 0%) to 1×10^{17} cm^{-3} (O/C = 1%). However, with gradual increase in oxygen concentration, the uncompensated acceptor concentration shows a trend of first increasing and then decreasing, reaching a maximum at O/C = 4% ($N_a - N_d = 3.9 \times 10^{17}$ cm^{-3}). When oxygen is in the plasma, oxygen may change the decomposition path of the gas phase precursor (B_2H_6) just like promoting the cracking of methane, which is conducive to formation of boron active species, resulting in a gradual increase in boron doping concentration under the condition O/C = 1%–4%. In the case of moderate oxygen content in diamond, stable boron–oxygen complexes can be formed with negative formation energy[46] (e.g., BOO, BOBB and BBOBB complexes) and increasing boron concentration, resulting in a higher boron concentration at O/C = 4% than at O/C = 0%. Direct competition for the doping of oxygen and boron reduces boron incorporation at higher oxygen levels.[20] These results demonstrate the precise tunability of boron doping concentrations through strategic addition of oxygen.

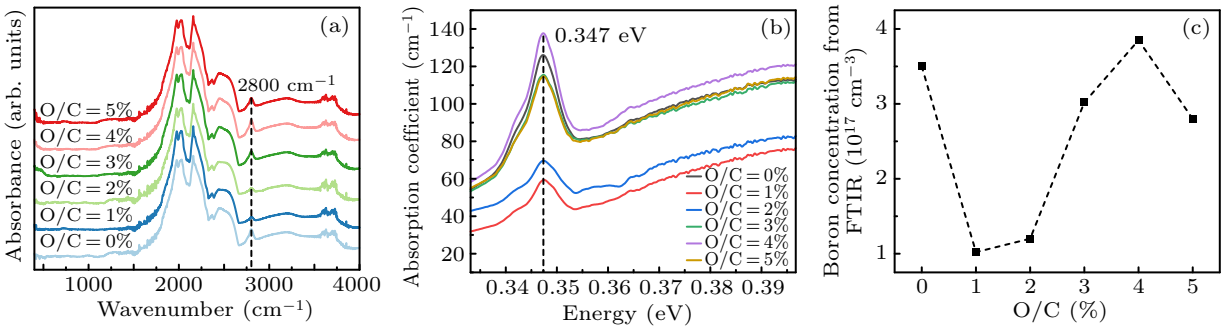


Fig. 6. FTIR absorption spectra of boron-doped diamond films: (a) an absorption peak related to boron appears in the FTIR spectrum at 2800 cm^{-1}; (b) the corresponding absorption coefficient versus energy. (c) The calculated boron concentration in diamond films.

Figure 7 shows the PL spectra of boron-doped diamond films recorded at 10 K using a 213 nm laser to analyze the boron doping level and other defects. Figure 7(a) shows exciton recombination with the different phonon replicas in the PL spectra of the diamond film in the near-bandgap region: the recombination of a boron-bound exciton with a TO phonon and an OΓ phonon (BE^{TO+O}) at 5.06 eV, the recombination of a boron-bound exciton with a TO phonon (BE^{TO}) at 5.22 eV, the recombination of a free exciton with a TO phonon (FE^{TO}) at 5.27 eV and the recombination of an exciton bound to boron without a phonon (BE^{NP}) at 5.35 eV.[47,48] The boron acceptor concentration can be calculated through the ratio between the BE^{TO} and FE^{TO} recombination intensities[49]

$$[\mathrm{B}] = 3.5 \times 10^{16} \frac{I_{\mathrm{BE}}^{\mathrm{TO}}}{I_{\mathrm{FE}}^{\mathrm{TO}}}\ (\mathrm{cm}^{-3}). \tag{2}$$

The estimated boron acceptor concentration in diamond film is plotted in Fig. 7(b). The boron acceptor concentrations derived from boron-bound excitonic intensity ratios exhibit striking alignment with FTIR quantification, confirming the non-monotonic influence of oxygen on doping efficiency. Compared with the single boron-doped diamond film, trace oxygen inhibits boron doping efficiency, and the boron acceptor concentration decreases from 1.1×10^{17} cm^{-3} (O/C = 0%) to 6.5×10^{16} cm^{-3} (O/C = 1%). With gradual increase in

the oxygen concentration, the boron acceptor concentration increases first and then decreases, reaching a maximum at O/C = 4%, as shown in the results obtained by FTIR ([B] = 1.2×10^{17} cm^{-3}). Crucially, the FWHM of the FE^{TO} peak serves as a sensitive metric of crystalline quality,[50] where reduced FWHM values directly correlate with a lower defect density. Diamond films at O/C = 1% and 4% demonstrate dramatically narrowed FE^{TO} peaks (FWHM ∼ 20 meV) compared with oxygen-deficient or excessive samples (FWHM ∼ 26 meV). This can be verified by the AFM and XRD results, and the lattice quality is improved in this condition.

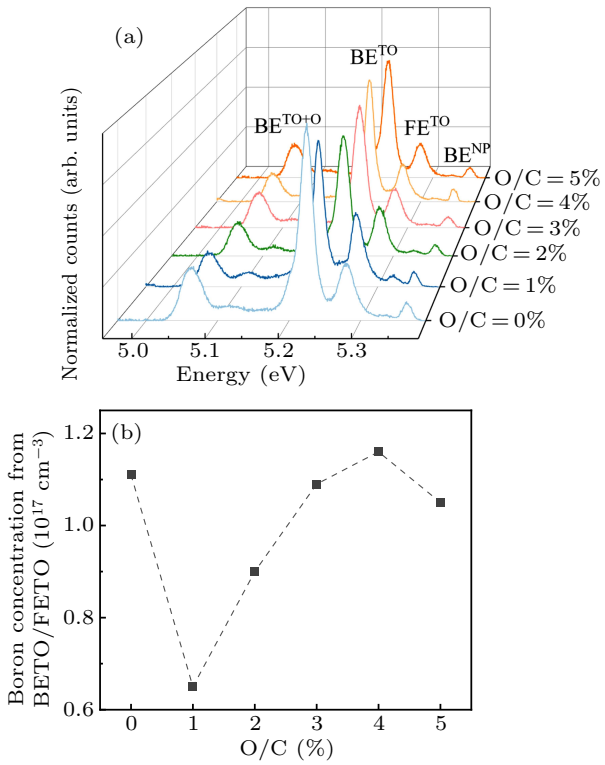


Fig. 7. (a) PL spectra of diamond films recorded at 10 K using a 213 nm laser. Two main peaks are observed in the near-bandgap region: BE^{TO} and FE^{TO}. (b) The calculated boron concentration in diamond films.

We continued to investigate defects in boron-doped diamond films by recording PL spectra in the range 250–700 nm (1.77–4.96 eV) using a 213 nm laser at 10 K, as shown in Fig. 8(a). The spectrum of each sample is normalized using the FE^{TO} peak. Beyond the dominant excitonic features, PL reveals multiple defect-related bands critical for quality assessment. The spectrum exhibits four broad emissions at 4.7 eV, 3.5 eV, 2.9 eV and 2.3 eV, accompanied by narrow peaks at 3.18 eV and 2.15 eV. Among these, the 4.7 eV (270 nm) band corresponds to a substitutional nitrogen donor[42] and the 3.5 eV emission indicates nitrogen incorporation.[51] The characteristic A-band (2.9 eV) signifies dislocation density or sp^2 bonds.[52] The green band (2.3 eV) originates from donor (nitrogen)–acceptor (boron) pairs decorating dislocations.[47] Here we focus on the broad band at 4.7 eV (270 nm). We plot the intensity of the peak at 4.7 eV in Fig. 8(b) and compare it with variation in NV centers (Fig. 5(b)). It can be seen that the density of defects corresponding to 4.7 eV is relatively large under single-boron doping (O/C = 0%) and excess oxygen (O/C = 5%), and the best result is shown at O/C = 1%, which is consistent with the change of NVs. However, when O/C = 1%–3%, the 4.7 eV peak intensity gradually increases instead of decreasing as shown for NV centers. Therefore, we speculate that this broad band is not only the effect of alternative N donors but also the boron–nitrogen complex. We note that the change in boron concentration is consistent with the peak intensity in the O/C range 0%–3%. The gradual increase in the 4.7 eV peak intensity may be attributed to the increasing boron concentration, while the decrease in peak intensity at O/C = 4% is due to the negligible NV concentration at this condition. Figure 8(c) shows the absorption spectra of boron-doped diamond films in the ultraviolet range, which have an obvious broad peak at 270 nm.[53] The absorption peaks are fitted and plotted in Fig. 8(d), and the inset shows variation of the absorption intensity with different oxygen concentrations. The change in the absorption peak intensity at 270 nm is almost the same as the peak intensity at 4.7 eV. The slight increase in absorption intensity at O/C = 2% further confirms the presence of boron.

Furthermore, we investigated the electrical properties of samples as shown in Fig. 9(a). Hall effects measurements were performed at room temperature using an HL5500PC Hall effects measurement system. Room-temperature Hall effect measurement confirms p-type conductivity in all diamond films, with carrier concentration and mobility exhibiting oxygen-dependent optimization (Fig. 9(a)). Hole concentration follows a non-monotonic trend: gradually increasing from 2.5×10^{14} cm^{-3} (O/C = 1%), reaching a peak of 1.5×10^{15} cm^{-3} when the O/C ratio is 4%; further increase in oxygen causes the hole concentration to decrease significantly. The variation of hole concentration with oxygen concentration in the range O/C = 1%–5% is consistent with the results obtained by FTIR and BE^{TO}. The increase in oxygen concentration regulates the acceptor concentration in the diamond film, and the number of carriers changes accordingly. We note that the boron monodoped sample is similar to the O/C = 1% condition, which seems to contradict the results for boron concentration extracted from FTIR and PL. This may be because trace oxygen reduces the boron ionization energy (0.22 eV at O/C = 0% and 0.19 eV at O/C = 2.5%);[40] this results in an increase in ionization efficiency and hole concentration when O/C = 1% and a reduction in the difference in hole concentration compared with the sample without oxygen. The change in mobility shows an optimal result in O/C = 1% and 4%, reaching 1200 cm$^2\cdot$V$^{-1}\cdot$s^{-1} (O/C = 1%) and 1400 cm$^2\cdot$V$^{-1}\cdot$s^{-1} (O/C = 4%), respectively, where oxygen mitigates lattice mismatch and suppresses the dominant scattering mechanisms. It can be seen from Fig. 9(a) that a lower mobility is measured at

O/C = 0% and O/C = 5%, which confirms that excessive defects prevail without optimal oxygen mediation. Oxygen plays a compensating role in boron-doped diamond by adding trace amounts of oxygen to repair the lattice mismatch, resulting in a significant improvement in mobility. Raman spectroscopy and XRD confirm the optimal lattice quality under this condition.

Currently, it is quite difficult to achieve P-type diamond with high hole concentration and mobility (or high crystal quality) simultaneously. In order to obtain high-quality P-type diamond, it is necessary to add very few doping atoms, resulting in a low carrier concentration. On the contrary, high doping will inevitably lead to poor crystal quality. Figure 9(b) summarizes the current results for mobility and carrier concentration of P-type boron-doped diamond with oxygen assistance at room temperature.[8,9,18,40,41,54–56] The two dashed lines in the figure represent a mobility of 1000 $cm^2 \cdot V^{-1} \cdot s^{-1}$ and a carrier concentration of 1×10^{15} cm^{-3}, respectively, so it can be seen that all results are located on the left of and below the lines. Our result achieves a mobility of 1400 $cm^2 \cdot V^{-1} \cdot s^{-1}$ and a carrier concentration of 1.5×10^{15} cm^{-3} (O/C = 4%) which is an excellent result compared with all previous studies while simultaneously achieving high hole concentration and mobility. This further improves the material performance of boron-doped diamond, which shows promising application prospects in high-voltage power devices.

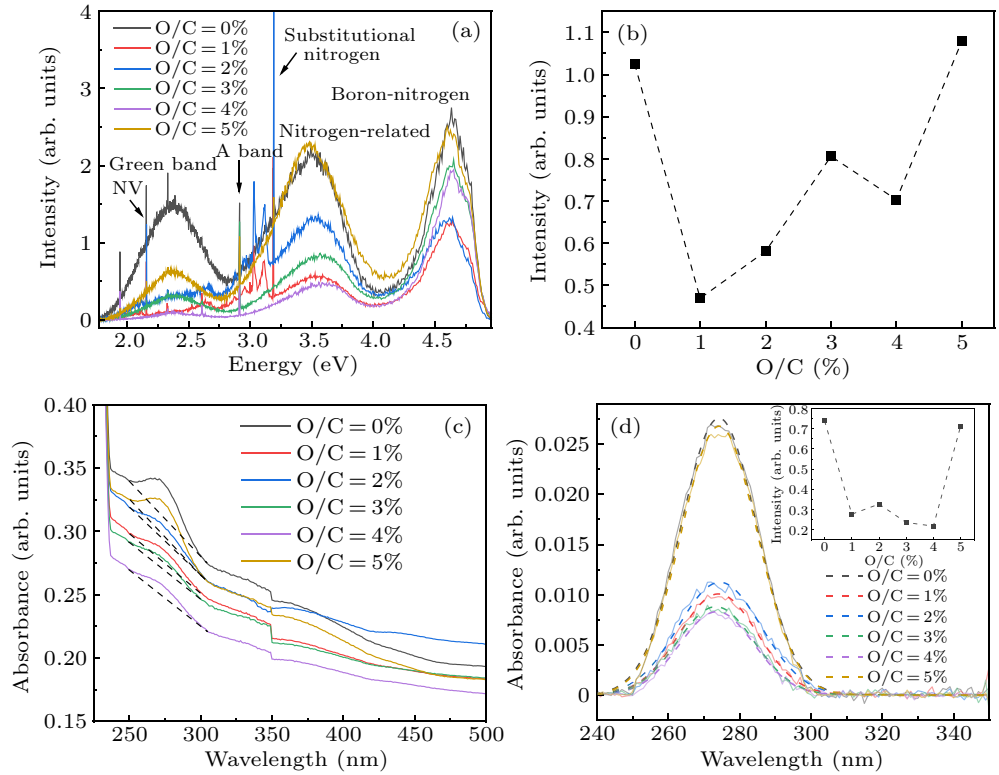


Fig. 8. Low-temperature PL and absorption spectra are used to analyze defects in boron-doped diamond films: (a) PL spectra in the range of 250–700 nm (1.77–4.96 eV) at 10 K; (b) the intensity of the peak at 4.7 eV (270 nm); (c) absorption spectra in the ultraviolet range; (d) the 270 nm absorption peak is fitted and the change of absorption intensity with O/C is plotted.

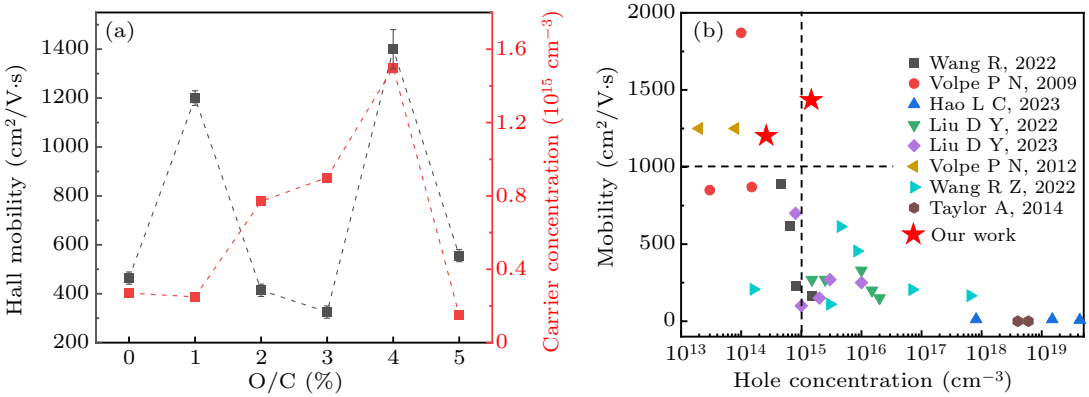


Fig. 9. Electrical properties of boron-doped diamond films at room temperature with increasing O/C gas ratio: (a) hole concentration and mobility; (b) the mobility of boron-doped diamond samples as a function of hole concentration in the literature.

4. Conclusion

In summary, modulation of the properties of lightly boron-doped diamond by trace oxygen was systematically investigated for an O/C range of 0% to 5% during MPCVD growth of diamond films. It was found that a proper amount of oxygen was beneficial to improving crystal quality, increased growth rate, enhanced boron doping efficiency, balanced boron doping stress and improved electrical properties of boron-doped diamond films. As the O/C ratio increased, oxygen also showed a regulatory effect on impurity defects. For samples grown at an oxygen concentration of 1%–4%, a high surface quality was observed by means of a low density of surface defects, while high crystalline quality was also demonstrated by Raman spectroscopy and XRD. When O/C = 4%, an advanced level of diamond material with both high hole concentration (1.5×10^{15} cm^{-3}) and high mobility (1400 cm$^2\cdot$V$^{-1}\cdot$s^{-1}) was realized, achieving excellent results in the field of boron-doped diamond, demonstrating the availability of the material for high-performance diamond-based electronic devices. In addition, we analyzed the characteristic peaks that appeared in both the low-temperature PL spectrum and absorption spectrum, and it was explained that the characteristic peak at 4.7 eV (270 nm) may correspond to the boron–nitrogen complex, supplementing the effect of boron-doped diamond on defect formation.

Acknowledgement

This work was supported by the National Natural Science Foundation of China (Grant Nos. 62274084 and 62574106).

References

[1] Isberg J, Hammersberg J, Johansson E, *et al*. 2002 *Science* **297** 1670
[2] Tallaire A, Brinza O, Mille V, *et al*. 2017 *Adv. Mater.* **29** 16
[3] Teraji T 2015 *J. Appl. Phys.* **118** 115304
[4] Liu D Y, Hao L C, Chen Z A, *et al*. 2020 *Appl. Phys. Lett.* **117** 022101
[5] Lee K W and Pickett W E 2004 *Phys. Rev. Lett.* **93** 237003
[6] Xu J, Yokota Y, Wong R A, *et al*. 2020 *J. Am. Chem. Soc.* **142** 2310
[7] Catalan F C I, Anh L T, Oh J, *et al*. 2021 *Adv. Mater.* **33** 2103250
[8] Wang R, Peng B, Bai H, *et al*. 2022 *Mater. Lett.* **322** 132345
[9] Volpe P N, Pernot J, Muret P, *et al*. 2009 *Appl. Phys. Lett.* **94** 092102
[10] Mortet V, Pernot J, Jomard F, *et al*. 2015 *Diam. Relat. Mater.* **53** 29
[11] Yap C M, Ansari K, Xiao S, *et al*. 2018 *Diam. Relat. Mater.* **88** 118
[12] Ding M, Liu Y, Lu X, *et al*. 2019 *Appl. Phys. Lett.* **114** 162901
[13] Imanishi S, Kudara K, Ishiwata H, *et al*. 2020 *IEEE Electron. Device Lett.* **42** 204
[14] Hao L C, Shen Y, Yang X D, *et al*. 2019 *J. Phys. D: Appl. Phys.* **53** 075107
[15] Issaoui R, Tallaire A, Mrad A, *et al*. 2019 *Phys. Status Solidi A* **216** 1900581
[16] Issaoui R, Achard J, William L, *et al*. 2019 *Diam. Relat. Mater.* **94** 88
[17] Fan K K, Tang K, Zhang M, *et al*. 2023 *Comp. Mater. Sci.* **222** 112113
[18] Hao L C, Chen Z A, Liu D Y, *et al*. 2023 *Chin. Phys. B* **32** 038101
[19] Bogdanov S A, Vikharev A L, Drozdov M N, *et al*. 2017 *Diam. Relat. Mater.* **74** 59
[20] Zhao G Y, Tang K, Teng Y, *et al*. 2024 *J. Mater. Res.* **39** 1313
[21] Frenklach M and Wang H 1991 *Phys. Rev. B* **43** 1520
[22] Bachmann P K, Leers D and Lydtin H 1991 *Diam. Relat. Mater.* **1** 1
[23] Lee N and Badzian A 1997 *Diam. Relat. Mater.* **6** 130
[24] Tallaire A, Kasu M, Ueda K, *et al*. 2008 *Diam. Relat. Mater.* **17** 60
[25] Friel I, Clewes S L, Dhillon H K, *et al*. 2009 *Diam. Relat. Mater.* **18** 808
[26] Ashkinazi E E, Khmelnitskii R A, Sedov V S, *et al*. 2017 *Crystals* **7** 166
[27] Chernov A A 1977 *J. Cryst. Growth* **42** 55
[28] Fiori A and Teraji T 2017 *Diam. Relat. Mater.* **76** 38
[29] Lloret F, Eon D, Bustarret E, *et al*. 2018 *Nanomaterials* **8** 814
[30] Ando T, Yamamoto K, Ishii M, *et al*. 1993 *J. Chem. Soc. Faraday Trans.* **89** 3635
[31] Seki Y, Hoshino Y and Nakata J 2021 *J. Appl. Phys.* **129** 195702
[32] Chu P K and Li L 2006 *Mater. Chem. phys.* **96** 253
[33] Liu Z, Fu J, Liu Z, *et al*. 2019 *Mater. Lett.* **240** 233
[34] Rouzbahani R, Nicley S S, Vanpoucke D E P, *et al*. 2021 *Carbon* **172** 463
[35] Fan Q H, Fernandes A, Pereira E, *et al*. 1998 *J. Appl. Phys.* **84** 3155
[36] Ichikawa K, Shimaoka T, Kato Y, *et al*. 2020 *J. Appl. Phys.* **128** 155302
[37] Hu X J, Shen Y G, Hao X P, *et al*. 2009 *Diam. Relat. Mater.* **18** 210
[38] Samudrala G K, Tsoi G, Stanishevsky A V, *et al*. 2011 *High Pressure Res.* **31** 388
[39] Hetzl M, Wierzbowski J, Hoffmann T, *et al*. 2018 *Nano Lett.* **18** 3651
[40] Liu D Y, Hao L C, Zhao W K, *et al*. 2022 *Chin. Phys. B* **31** 128104
[41] Liu D Y, Tang K, Zhu S M, *et al*. 2023 *Chin. Phys. B* **32** 118102
[42] Fernández-Lorenzo C, Araújo D, González-Mañas M, *et al*. 2012 *J. Cryst. Growth* **353** 115
[43] Chevallier J, Lusson A, Ballutaud D, *et al*. 2001 *Diam. Relat. Mater.* **10** 399
[44] Demlow S N, Grotjohn T A, Hogan T, *et al*. 2010 *MRS Proceedings* **1282** 67
[45] Collins A T and Williams A W S 1971 *J. Phys. C: Solid State Phys.* **4** 1789
[46] Zhang M, Tang K, Wu K P, *et al*. 2023 *Comp. Mater. Sci.* **216** 111867
[47] Kadri M, Araujo D, Wade M, *et al*. 2005 *Diam. Relat. Mater.* **14** 566
[48] Omnès F, Muret P, Volpe P N, *et al*. 2011 *Diam. Relat. Mater.* **20** 912
[49] Rouzbahani R, Pobedinskas P, Donatini F, *et al*. 2024 *Carbon* **221** 118923
[50] Ghodbane S, Omnès F and Agnès C 2010 *Diam. Relat. Mater.* **19** 273
[51] Yelisseyev A P and Nadolinny V A 1995 *Diam. Relat. Mater.* **4** 177
[52] Araújo D, Paz Alegre M A, García A J, *et al*. 2011 *Phys. Status Solid C* **8** 1366
[53] Vins V G, Yelisseyev A P, Smovzh D V, *et al*. 2018 *Diam. Relat. Mater.* **86** 79
[54] Volpe P N, Arnault J C, Tranchant N, *et al*. 2012 *Diam. Relat. Mater.* **22** 136
[55] Wang R Z, Yan X L, Peng B, *et al*. 2022 *J. Synth. Cryst.* **51** 893
[56] Taylor A, Fekete L, Hubík P, *et al*. 2014 *Diam. Relat. Mater.* **47** 27